HHS Public Access

Author manuscript

Neurobiol Dis. Author manuscript; available in PMC 2020 November 01.

Published in final edited form as:

Neurobiol Dis. 2020 November ; 145: 105083. doi:10.1016/j.nbd.2020.105083.

Detection of neurophysiological features in female R255X MeCP2 mutation mice

Hong-Wei Dong[a,b], **Kirsty Erickson**[a,b], **Jessica R. Lee**[a,b], **Jonathan Merritt**[a,b], **Cary Fu**[a,b], **Jeffrey L. Neul**[a,b,*]

[a]Department of Pediatrics, Division of Neurology, Vanderbilt University Medical Center, Nashville, TN 37212, USA

[b]Vanderbilt Kennedy Center, Vanderbilt University Medical Center, Nashville, TN 37203, USA

Abstract

Rett syndrome (RTT) is a severe neurodevelopmental disorder (NDD) that is nearly always caused by loss of function mutations in *Methyl-CpG-binding Protein 2* (*MECP2*) and shares many clinical features with other NDD. Genetic restoration of *Mecp2* in symptomatic mice lacking MeCP2 expression can reverse symptoms, providing hope that disease modifying therapies can be identified for RTT. Effective and rapid clinical trial completion relies on well-defined clinical outcome measures and robust biomarkers of treatment responses. Studies on other NDD have found evidence of differences in neurophysiological measures that correlate with disease severity. However, currently there are no well-validated biomarkers in RTT to predict disease prognosis or treatment responses. To address this, we characterized neurophysiological features in a mouse model of RTT containing a knock-in nonsense mutation (p.R255X) in the *Mecp2* locus. We found a variety of changes in heterozygous female $Mecp2^{R255X/X}$ mice including age-related changes in sleep/wake architecture, alterations in baseline EEG power, increased incidence of spontaneous epileptiform discharges, and changes in auditory evoked potentials. Furthermore, we identified association of some neurophysiological features with disease severity. These findings provide a set of potential non-invasive and translatable biomarkers that can be utilized in preclinical therapy trials in animal models of RTT and eventually within the context of clinical trials.

Keywords

Neurodevelopmental disorders; Electroencephalogram (EEG); Event-related potential (ERP); Rett syndrome; Neurophysiological features; Biomarkers

1. Introduction

Rett syndrome (RTT) is a severe neurodevelopmental disorder (NDD) that predominantly affects females and is found in ~1:10,000 female births (Laurvick et al., 2006). RTT is characterized by a distinctive pattern of disease, with apparently normal early development

*Corresponding author at: 230 Appleton Place, Nashville, TN 37203, USA, jeffrey.l.neul@vumc.org (J.L. Neul).

for the first ~6 months of age, developmental stagnation, and then a period of regression with loss of acquired volitional hand skills and spoken language, onset of repetitive hand movements, and gait problems (Neul et al., 2010). Affected individuals often develop clinical features such as seizures (Tarquinio et al., 2017), breathing irregularities (Tarquinio et al., 2018) and autonomic dysfunction (McCauley et al., 2011). Loss of function mutations in the X-linked gene *Methyl-CpG-binding Protein 2* (*MECP2*), which encodes the transcriptional regulator protein MeCP2, are the major cause of RTT (Amir et al., 1999; Cuddapah et al., 2014). Hundreds of *MECP2* mutations have been found to cause RTT, among which eight common point mutations in *MECP2* (R106W, R133C, T158M, R306C, R168X, R255X, R270X, R294X) account for over 60% of RTT cases (Cuddapah et al., 2014; Neul et al., 2008). To better understand the disease pathophysiology and seek effective treatment, a mouse model containing a knock-in nonsense mutation (p.R255X) in the *Mecp2* locus ($Mecp2^{R255X}$) has been created (Pitcher et al., 2015). This mouse model displayed similar behavioral deficits to mice completely lacking the bulk of *Mecp2* coding sequence (*Mecp2* null mice). However, the neurophysiological phenotypes in the $Mecp2^{R255X}$ mice have not been investigated.

Neurophysiological features such as electroencephalography (EEG) and event-related potential (ERP) are used to evaluate neural circuit changes in schizophrenia, NDDs, and autism (Featherstone et al., 2015; Gandal et al., 2010; Gandal et al., 2012; Roberts et al., 2010; Uhlhaas and Singer, 2010; Ward et al., 2019) because they are non-invasive, well tolerated (even in severely disabled NDD), sensitive, reliable, and reproducible (Light and Swerdlow, 2015). Furthermore, it is possible to evaluate neurophysiological features using parallel methods in preclinical animal models (especially mouse) and in people, allowing for easy translation of findings. For example, parallel neurophysiological assessments have been done in Fragile X Syndrome (FXS) (Lovelace et al., 2018; Sinclair et al., 2017b; Wen et al., 2019), a common genetic NDD. EEG recordings in people with FXS showed reduced habituation of N1 amplitude of auditory event-related potential (AEP) (Ethridge et al., 2016; Van der Molen et al., 2012), increased baseline gamma band power (Ethridge et al., 2017; Ethridge et al., 2019; Wang et al., 2017) and altered auditory induced neural oscillation (Ethridge et al., 2017; Ethridge et al., 2019), which have also been observed in mouse models of FXS (Jonak et al., 2020; Lovelace et al., 2016; Lovelace et al., 2018; Wen et al., 2019). Correlations between neurophysiological features and disease severity in FXS have been established in both human and mice, suggesting that neurophysiological features can serve as biomarkers to predict disease progress and severity (Ethridge et al., 2016; Ethridge et al., 2019; Wen et al., 2019). Recent work in FXS mice found that a specific neurophysiological response (increased gamma oscillations) to baclofen predicted short-term memory improvement after chronic baclofen treatment, supporting the utility of neurophysiological features as biomarkers predictive of treatment response (Sinclair et al., 2017a).

EEG and ERP recordings in individuals with RTT suggested that alterations in brain activity are associated with behavioral and cognitive deficits (Ammanuel et al., 2015; Foxe et al., 2016; Key et al., 2019; LeBlanc et al., 2015; Roche et al., 2019; Stauder et al., 2006). Some electrophysiological features evaluated in people, such as basal EEG and ERP, have been preliminarily investigated in RTT animal models (Goffin et al., 2012;

Goffin et al., 2014; LeBlanc et al., 2015; Liao et al., 2012; Wither et al., 2012). *Mecp2* NULL heterozygous female mice and RTT individuals exhibited a similar decrease in visual evoked potential (VEP) amplitude and displayed a deficit in discriminating smaller patterns (LeBlanc et al., 2015). EEG resting delta power was elevated in individuals with RTT and showed correlation with the severity of symptoms (Roche et al., 2019). Gamma power in response to the mother's voice was decreased in people with RTT (Peters et al., 2015). In mouse models of RTT, there was an increase in resting high gamma power and dramatically decreased event-related power in all frequencies in $Mecp^{T158A/Y}$ mice (Goffin et al., 2012), but no change in resting delta power in $Mecp^{NULL/+}$ female mice (Wither et al., 2012). Interestingly, the oscillations of delta cycles were positively correlated with brain MeCP2 content (Wither et al., 2013). The decreased auditory amplitude and prolonged latency of AEP observed in people with RTT (Stauder et al., 2006) were also observed in $Mecp^{T158A/Y}$ male mice (Goffin et al., 2012; Goffin et al., 2014). However, contradictory results were reported in $Mecp^{NULL/+}$ female mice (Liao et al., 2012). Overall, parallel studies on the neurophysiological features between people with RTT and mouse models of RTT, and correlations between neurophysiological features and disease severity, remain limited. Thus, there is an ongoing need for more extensive characterization with an eye towards translatability between human and animal models to enable the development of non-invasive biomarkers that could be used to predict treatment response or serve as early efficacy biomarkers in interventional trials. To address this need, we evaluated a variety of neurophysiological features in a valid disease model of RTT (heterozygous female $Mecp2^{R255X/X}$) at a variety of ages and with a focus on translatable features such as EEG and ERP and clinically relevant features commonly present such as sleep/wake disturbance (Ellaway et al., 2001; Young et al., 2007) and epileptiform activity and seizures (Tarquinio et al., 2017) to identify neurophysiological features that correlate with age and disease severity.

2. Methods

All experimental mice were generated from $Mecp2^{R255X/X}$ (Jackson Laboratory #012602, $Mecp2^{tm1.1Irsf/J}$) animals that have been back-crossed > 20 generations to C57BL6/J (Pitcher et al., 2015). Littermate wild-type female animals were used as controls. All procedures used in this study adhered to the published guidelines of the National Institutes of Health and were approved by the Institutional Animal Care and Use Committee at Vanderbilt University Medical Center. Mice were maintained in an AAALAC accredited facility in 12 h light/dark cycles and fed standard mouse chow. Food and water were provided ad libitum. EEG recordings were performed on $Mecp2^{R255X/X}$ female mice at the young age of 5–8 postnatal weeks (n = 10, termed the "Young" cohort) and old age of postnatal 20–24 weeks (n = 18, the "Old" cohort). Wildtype littermate female animals (n = 11 for the Young and n = 18 for the Old) served as control.

2.1. EEG headmount implantation

Animals were anesthetized with isoflurane and a subcutaneous injection of ketoprofen (10 mg/kg) was applied for analgesia. After animals were secured in a stereotaxic apparatus, a midline sagittal incision was made along the scalp to expose the skull. An EEG/EMG headmount (#8201-SS, Pinnacle Technology Inc.) was positioned along the middle of the

exposed skull with the front edge 2.0 mm anterior to bregma. A dental drill was used to drill 1 mm diameter burr holes at the four attachment sites of the headmount (two front burr holes: +1.9 mm anterior to bregma and ± 1.8 mm lateral to middle line; two back burr holes: 4.0 mm posterior to bregma and ± 1.8 mm lateral to middle line). Four stainless steel screw electrodes (#8209, Pinnacle Technology Inc.) measuring 2.5 mm in length were threaded through the burr holes (right parietal for EEG1, right frontal for EEG2, left frontal and left parietal served for ground and reference). Two stainless wires mounted to the tail of the headmount were inserted into the two side trapezius muscles for EMG recording. The electrodes and base of the headmount were covered in fast-setting dental cement. Mice were placed on a heating pad to help recovery from anesthesia and additional doses of ketoprofen were administered 24 h later for continuous analgesia after surgery. Mice were individually housed, returned to the vivarium and monitored accordingly until the day of EEG recordings.

2.2. Data collection

After a minimum of one-week recovery from surgery, animals were housed individually in transparent chambers for continuous EEG data acquisition. EEG recordings were collected from freely moving mice with unrestricted access to food/water and maintained under 12-h dark-light cycles. EEG headmounts were rigidly connected to a preamplifier system (#8202-SL, Pinnacle Technology Inc., Lawrence, KS). The signals were pre-amplified 100× with initial high pass filter of 0.5 Hz. Then the signals were routed to an 8401 conditioning/acquisition system (Pinnacle Technology, Inc., Lawrence, KS) via a tether and low-torque commutator (Part #8408, Pinnacle Technology, Inc., Lawrence, KS), in which the amplifier/conditioning unit provided an additional 50× signal amplification, additional high-pass filtering, and an 8th order elliptic low pass filter (0.5 to 200 Hz). The signals were sampled at 400 Hz, digitized using a 14bit A/D converter and routed to a PC based acquisition and analysis software package via USB. All EEG data was obtained using Sirenia Software from Pinnacle Technologies, Inc. Animal activity was monitored using an online camera and data was stored for offline analysis. AEP were evoked during EEG recordings. Auditory stimuli consisted of a series of 200 white-noise pips (10-ms duration, 0.25 Hz frequency) generated from a commercially available acoustic stimulus system (San Diego Instruments) with speakers positioned above the recording chamber. Sound delivery was synchronized with EEG recordings using a TTL pulse to mark the onset of each sound in a train. Stimuli were calibrated using a sound pressure meter at 80+/− 3 dB SPL.

2.3. Data analysis

2.3.1. Evaluation of sleep/wake cycles—EEG waveforms were analyzed using Sirenia sleep software package (Pinnacle Technology Inc., Lawrence, KS) to evaluate animal activity state. All recorded EEG waveforms in 20 h were scored as 10s epochs of wake state (Wake), non-rapid eye movement sleep state (NREM), or rapid eye movement sleep state (REM) by a blinded scorer. Animal movement state was first determined as wake (continuous movement) and sleep (prolonged periods of no movement) state by reviewing captured video. The sleep state was further classified as NREM or REM sleep state according to EEG appearance. The synchronous EMG and video were applied for further confirmation of wake-inactive states. In 10s epochs where transitions between behavioral

states occurred, the EEG epoch was scored as the EEG state that was > 5 s (dominant). According to the score, duration, average length of each bout and the number of bouts of all three states were calculated and analyzed. Because AEP was normally observed between 11:00 am to 2:00 pm, we analyzed mouse sleep and wake cycles by setting 2 pm to 6 pm and 7 am to 11 am as light cycle and 7 pm to7 am as dark cycle.

2.3.2. Evaluation of EEG power and AEP—The saved EEG data was imported into MATLAB (MathWorks, Inc). For resting EEG frequency analysis, periods were classified as Wake, NREM or REM and segmented into 10s intervals for analysis. Spectral plots were generated with the Fast Fourier Transformation (FFT) function with rectangular binning of 10s, 50% window overlap and a spectral resolution of 0.2 Hz. The average power (μV^2/Hz) was calculated from 1 to 100 Hz. Power was then further binned into standard frequency bands: Delta (2–4 Hz), Theta (4–8 Hz), Alpha (8–12 Hz), Beta (12–30 Hz), Gamma (30–55 Hz) and high Gamma (65–100 Hz). For comparisons across the individuals, the spectral power was normalized by the total power under 0–100 Hz. In order to investigate the potential role of abnormal neural network activities in RTT mice and the effect of neural noise in shaping the power spectrum seen in these mice, the 1/f slope of the power spectrum was calculated in the 2–24 Hz frequency range via linear regression in log-log scale. For AEP analysis, EEG data was exported as −100 ms to 500 ms epoch relative to the auditory stimulation. Signals from −100 ms to 0 before the stimulation were taken as the baseline. Recordings across 200 trials were averaged from each mouse. Trials containing activity over 2 SD of the mean of the 200 trials were rejected. Peak components were extracted from grand-average waveforms as follows: P1 (positive deflection between 10 and 70 ms), N1(negative deflection between 50 and 150 ms) and P2 (positive deflection between 100 and 350 ms). Event-related power of single AEP responses was calculated by the −100 ms to 500 ms epoch relative to the auditory stimulation. For each epoch, inter-trial coherence (ITC) were calculated using Morlet wavelets in 100 linearly spaced frequency bins between 1 and 100 Hz, with wavelet cycles of 6. ITC at frequency bands of Delta (2–4 Hz), Theta (4–8 Hz), Alpha (8–12 Hz), Beta (12–30 Hz), Gamma (30–55 Hz) and high Gamma (65–100 Hz) were calculated in wildtype and mutant animals respectively.

2.3.3. Analysis of epileptiform discharge events—EEG traces were exported to Clampfit 10 and bandpass filtered at 0.5–20 Hz. Waveforms were characterized as epileptiform by their spike-wave appearance with peak voltage of at least 1.5-fold background, occurring in a rhythmic train with frequency between 6 and 10 Hz and duration of at least 0.5 s. Epileptiform discharge was first automatically detected and then visually confirmed. EEG samples were quantified during 8:00 am to 11:00 am with the cumulative discharges per hour reported for each mouse.

2.3.4. Evaluation of severity of disease—Overall severity scoring of the mice was conducted using the “Bird” scoring system, which is based on visual inspection of key phenotypes observed in *Mecp2* mutant mice that include general condition, activity, gait, hindlimb clasping, tremor, and breathing regularity (Guy et al., 2007). Each phenotypic domain is rated on a three-point scale (0-absent, 1-mildly present, and 2-severely present), and a total score is used as a measure of the overall phenotypic severity. Bird score was

evaluated on the day before EEG recording. All scores acquired from six categories in each animal were summed to represent the overall phenotypic severity.

2.4. Data statistics

Statistics and graphical representation of data was performed using Prism 8.1 (San Diego, CA). Data were expressed as mean ± SEM. Comparisons between genotypes were estimated using two tails Student unpaired *t*-test and Mann-Whitney *U* test based on whether the data passed normality test (Shapiro-Wilk test, $p < 0.05$ was set as rejection of normality). Bonferroni-Holm adjustment of *p*-value was applied in each study. Spearman's rho correlations were performed to investigate the associations between neurophysiological features and disease severity. $p < 0.05$ was set as significant difference and $p < 0.1$ was considered as the trend towards alteration. In the text, wildtype animals were termed as WT and *Mecp2*$^{R255X/X}$ animals were termed as MUT.

3. Results

3.1. Sleep/wake cycle is disrupted in Mecp2$^{R255X/X}$ female mice

Fig. 1A shows representative tracing of the EEG features observed in the three different sleep/wake states (Wake [1]; NREM [2]; and REM [3]) in an animal at 20 weeks old, in which the Wake period displays rapid, low and irregular EEG waveform, NREM shows slow and high amplitude EEG waveform, and the REM period is characterized by rapid, low amplitude, and relative rhythmic EEG waveform. Fig. 1B shows representative hypnograms during the total recording period, identifying the sleep/wake state on the y-axis. Over the entire recording period, *Mecp2*$^{R255X/X}$ female animals (MUT) showed decreased total time in REM state (Fig. 1C, $p < 0.05$, *t*-test) compared to littermate wild-type controls (WT), which was not related to the length of REM bouts (Fig. 1C2) but due to a decreased number of REM bouts (Fig. 1C3, $p < 0.05$, Mann-Whitney *U* test). Interestingly, these differences between WT and MUT in REM state were only observed in the light cycle (Fig. 1D1–D3). Additionally, during the light cycle, the total awake time of MUT animal was longer than the WT (Fig. 1D1, $p < 0.05$, t-test), while this difference was mainly caused by the trend towards increased average length of Wake bouts (Fig. 1D2, WT vs. Mut, 142.3 ± 71.7 s vs.182.1 ± 63.5 s, $p = 0.091$, t-test) but not the number of bouts (Fig. 1D3. WT vs. Mut, 79 ± 41.3 vs. 70.1 ± 22.1, $p = 0.47$, t-test). There was no difference of the light cycle NREM state total time, average length of bouts, or and bout number between the genotypes (Fig. D1–D3). During the dark cycle there were no significant changes between genotypes in any of the observed parameters (Fig. 1E1–E3). Next, we compared all these parameters between genotypes in young animals (5–8 weeks, Table 1). The only change observed between genotypes in these young animals was a decreased number of light cycle REM bouts in Mut animals (Table 1, $p < 0.05$, Mann-Whitney U test) that drove the decreased number of REM bouts in the total observed period (Table 1, $p < 0.05$, Mann-Whitney U test). This decrease did not significantly change REM duration after Bonferroni correction. Looking at changes in these sleep/wake cycles over developmental age, we observed that there was no difference in light cycle Wake duration in the Young cohort, however there was a difference in the Old cohort (Fig. 1F1). In contrast, we observed a parallel increase in light cycle REM duration (Fig. 1F2) and bouts (Fig. 1F3) in both WT (duration, $p < 0.001$, *t*-test; bouts $p = 0.06$,

Mann-Whitney U test) and Mut (duration, $p < 0.01$, *t*-test; bouts p < 0.01, Mann-Whitney U test). However, as mentioned above, while REM bout number was different between the genotypes in both the Young and Old cohort, REM duration was only different between the genotypes in the Old cohort.

3.2. Mecp2$^{R255X/X}$ female mice have alterations in resting EEG power

Resting EEG power was calculated both from parietal brain region and frontal brain region of MUT and WT littermate mice by analyzing EEG frequency bands during periods of Wake, NREM, and REM states. Within the Old (20–24 wks old) cohort, animals of both genotypes showed distinct spectral patterns during different sleep/wake states, with increased power in high frequency bands during the Wake state, increased low frequency band power in NREM state, and decreased power in both high and low frequency bands in REM state compared to either Wake or NREM state (Supplemental Fig. 1). The power in each frequency was normalized by the total power under the curve (Fig. 2 A. B). We compared the differences of each power bands between genotypes by the brain areas under three sleep/wake states, Wake (Fig. 2C–D), NREM (Fig. 2E–F) and REM (Fig. 2G–H). Delta power was increased in MUT animals in the Wake state in both the parietal (Fig. 2C, $p < 0.05$, t-test) and the frontal region (Fig. 2D, $P < 0.01$, t-test), in the frontal region during NREM (Fig. 2F, p < 0.01,t-test), and trend towards increase in MUT in the frontal region during REM (Fig. 2H, $p < 0.1$, t-test). Theta band power was increased in MUT in the parietal region during REM (Fig. 2G, p < 0.0, *t*-test). In contrast to the lower delta and theta power bands, alpha power was decreased in MUT under most circumstances, including in the parietal region during Wake (Fig. 2C, $p < 0.01$, t-test) and NREM (Fig. 2E, $p < 0.05$, t-test) and in the frontal region during NREM (Fig. 2F, $p < 0.001$,t-test) and REM (Fig. 2H, p < 0.01,t-test). High power bands (gamma or high gamma) showed a trend towards decrease in MUT animals in the parietal region during REM (Fig. 2G, $p < 0.1$,t-test), and in the frontal region during NREM (Fig. 2F, p < 0.1,t-test) and REM (Fig. 2H, p < 0.1, t-test). All other frequency bands were not different between genotypes. In contrast to the Old cohort, the Young Cohort (5–8 weeks, Table 2) revealed no significant difference between MUT and WT animals except a trend towards increased delta power and decreased alpha power in the frontal region during NREM (Table 2, p < 0.1). Fig. 2I shows the developmental progression of high gamma power in the parietal and frontal regions during the Wake state. We evaluated the relationship of high gamma power to overall phenotypic severity, as assessed using a standardized visual inspection scoring system (“Bird Score”, higher scores indicate increased severity). Within the parietal region, there is a strong correlation between increasing phenotypic severity and decreasing high gamma power in all sleep/wake states (Fig. 2J, Wake: $r = 0.54$, $p = 0.008$; Fig. 2K, NREM: $r = 0.59$, $p = 0.003$ and Fig. 2L, REM: $r = 0.62$, $p = 0.002$). In contrast, there was not a clear correlation between high gamma power and severity in the frontal region (Wake: $r = 0.17$, $p = 0.43$, NREM: $r = 0.36$, $p = 0.08$ and REM: $r = 0.30$, $p = 0.16$). Although delta and alpha power showed alterations in the old MUT animals, there was no correlation of these power bands and phenotypic severity (Data not shown).

Previous work in people with RTT used 1/f slope of the power spectrum between 2 and 24 Hz (log-log transformed) to investigate excitatory/inhibitory imbalance and the effect of

neural noise (Roche et al., 2019; Voytek et al., 2015), and found that people with RTT have a significantly more negative slope compared to typically developing controls. We conducted a similar analysis of the 1/f slope from the experimental animals (Fig. 3). In the Old cohort, we detected a more negative slope in MUT animals in most sleep/wake states of two brain regions (Fig. 3A, parietal: Wake, $p < 0.05$, NREM, $p < 0.01$; Fig. 3B, frontal: Wake, $p < 0.001$, NREM, $p < 0.001$ and REM, $p < 0.01$, *t*-test) and a trend towards decrease in REM state of parietal region ($p < 0.1$, Mann-Whitney *U* test). In contrast, there was no differences in 1/f slope in young animals, as seen by plotting the 1/f slope normalized to WT values (Fig. 3C, E, G). There is a clear developmental progression, with a larger slope observed in the frontal region during Wake (Fig. 3C, $p < 0.05$, Mann-Whitney U test) and REM (Fig. 3G, $p < 0.05$, Mann-Whitney U test) in Old animals compared to Young animals. In contrast, we did not observe a significant change in the slope during aging in the parietal region. Surprisingly, frontal 1/f slope was not associated with the phenotypic severity in any sleep/wake states (Fig. 3D, F, H), but parietal 1/f slope was correlated with severity during NREM (Fig. 3F, $r = 0.64$, $p = 0.003$) and REM (Fig. 3H, $r = 0.45$, $p = 0.02$).

3.3. Increased epileptiform discharges are present in Mecp2$^{R255X/X}$ female mice

Epileptiform discharges and seizures are common in people with RTT (Tarquinio et al., 2017), and spontaneous epileptiform discharges have been reported in male and female *Mecp2* deficient mice (D'Cruz et al., 2010; Lang et al., 2014; Wither et al., 2012; Wither et al., 2018). We investigated whether *Mecp2* R255X heterozygous female mutant mice also displayed epileptiform discharges. As shown in Fig. 4A–B, rhythmic spontaneous discharges at frequency of 6–10 Hz were observed in 9/10 MUT mice, compared to 0/11 in WT mice at the young age ($z = 2.73$, $p = 0.0064$, X^2 -test), as well as in 16/18 MUT mice, compared to 1/18 in WT mice at the old age ($z = 3.12$, $p = 0.0018$, X^2 -test). The average number of epileptiform discharges per hour in MUT mice in the Old cohort was significantly higher than in the Young cohort (Fig. 4C, $U = 3$, $z = -3.88$, $p = 0.0001$, Mann-Whitney U test), and correlated strongly with phenotypic severity (Fig. 4D, $r = 0.7$, $p = 0.0002$).

3.4. Mecp2$^{R255X/X}$ female mice have alterations in auditory evoked potentials

Auditory evoked potentials (AEP, Fig. 5A) have three distinct peaks with an initial small positive peak (P1), followed by a negative peak (N1) and a subsequent positive peak (P2) (Goffin et al., 2012). We investigated AEP difference between genotypes in parietal brain region. In Old MUT mice, N1 ($p < 0.01$), P2 ($p < 0.05$), and N1-P2 ($p < 0.01$, *t*-test, Fig. 5B) amplitudes were significantly decreased. AEP latency was delayed in MUT only in P2 ($p < 0.01$, t-test, Fig. 5C). Young MUT mice did not show any differences in AEP amplitudes or latency (Fig. 5D, Table 3), but a clear age-related decline of N1-P2 amplitude was observed in MUT ($p < 0.05$, t-test) that was not present in WT mice (Fig. 5D). AEP N1-P2 amplitude is negatively correlated with phenotypic severity (Fig. 5E, $r = 0.45$, $p = 0.02$) and with epileptiform discharges (Fig. 5F, $r = 0.66$, $p < 0.001$).

Finally, we performed time-frequency analysis of the AEP data in Young (Table 3) and Old animals (Data shown in Fig. 5B–C). Inter-trial phase coherence (ITC) assesses synchronized brain activity to auditory stimuli as a function of time and represents auditory-stimulus phase locked power. In Old animals (Fig. 5G), ITC immediately increased after the sound

stimulation across a wide range of frequency bands in both WT and MUT animals; however, MUT showed a decreased level of ITC compared to WT animals (Fig. 5H). MUT animals had smaller ITC compared to WT at theta ($p < 0.01$), alpha ($p < 0.01$), beta ($p < 0.01$) and gamma frequency bands (Fig. 5H, $p < 0.001$, t-test). Young mice did not show differences in ITC between MUT and WT animals (Fig. 5I1–I4). However, in MUT mice, a dramatic decrease of ITC at theta, alpha, beta and gamma bands was seen with aging (Fig. 5I1–I4, $p < 0.01$, t-test). Finally, ITC in the theta ($r = 0.50$, $p = 0.017$) and alpha ($r = 0.51$, $p = 0.015$) bands showed negative correlation with phenotypic severity, while ITC at beta ($r = 0.29$, $p = 0.178$) and gamma bands ($r = 0.34$, $p = 0.112$) did not (Fig. 5J1–J4, $N = 22$).

4. Discussion

This is the first study evaluating various neurophysiological features and their possibilities of serving as biomarkers in heterozygous female *Mecp2*$^{R255X/X}$ mice, a RTT mouse model containing a severe, common point mutation in *MECP2*. This work identified changes in sleep/wake cycle in *Mecp2*$^{R255X/X}$ mice, with increased wake time and reduced REM sleep during the light cycle. We found changes in the EEG power spectrum, specifically increased resting delta power and decreased alpha power, which led to increases of the negative 1/f slope in both wake and sleep (NREM and REM) states. In resting condition, *Mecp2*$^{R255X/X}$ mice also showed an increased incidence of spontaneous epileptiform discharges, similar to that previously reported (Lang et al., 2014; Wither et al., 2012). Additionally, we observed alterations in auditory evoked potential with prolonged peak latencies and decreased peak amplitudes, and decreased event-related phase locked power (ITC) across a wide range of frequency bands, similar to that seen in people with RTT or animal models (Foxe et al., 2016; Goffin et al., 2012; Goffin et al., 2014; Stauder et al., 2006). Specifically, the changes of neurophysiological features, such as 1/f slope, basal high gamma power, spontaneous epileptiform discharges, AEP amplitude (N1-P2) and auditory related phase locked theta and alpha power were correlated strongly with phenotypic severity, which provides the possibility of applying these neurophysiological features as biomarkers for evaluating disease progress, severity and predicting treatment responses.

Sleep disturbance is very common in individuals with RTT, with over 80% of affected people having sleep abnormalities including irregular sleep/wake patterns, frequent arousal during sleep, increased day time napping and increased sleep onset latency (Glaze et al., 1987; Nomura, 2005; Tarquinio et al., 2018; Young et al., 2007). The reported evaluations of sleep/wake patterns in mouse models lacking MeCP2 function varied depending on whether the studies were in heterozygous female or hemizygous male mice. Studies by Johnson et al. in male *Mecp2*$^{NULL/Y}$ mice reported increased wakefulness in the dark cycle, increased sleep latency, and increased duration of the longest bout of NREM state (Johnson et al., 2017). Using the same male hemizygous animals, Li et al. found increased sleep bouts with shorter duration (Li et al., 2015). To date, only one study has been conducted in heterozygous adult female *Mecp2*$^{NULL/+}$ mice, in which an increased amount of wake state periods in the light and dark cycles was observed with an increased length of each bout but decreased number of bouts (Wither et al., 2012). In this work, we found that most changes of the sleep pattern in *Mecp2*$^{R255X/X}$ female mice occurred during the light cycle including the decreased total REM time that was driven by the decreased number of REM

bouts and increased total wake time that reflected the trend towards increased average length of Wake bouts. A difference between the two studies was that Wither et al. performed the experiments using telemetry recording on Mecp2$^{Null/+}$ mice at age of 300–400 days, which was older than the experimental conditions outlined here (the oldest within 170 days). It is possible that *Mecp2*$^{R255X/+}$ will develop similar dark cycle abnormalities as observed in *Mecp2* $^{Null/+}$ as they age. Additionally, large inter-animal variations in the length of wake bouts in the WT control group prevented the observation of significant differences between the genotypes in this study. Interestingly, a strong relationship between sleep state, particularly REM sleep, and learning has been previously reported (Smith, 1996). Thus, the shortening of REM sleep time might decrease mouse learning capability and lead to observed cognitive dysfunction. The age-dependent quantitative differences and correlation with severity observed here in sleep/wake patterns in *Mecp2*$^{R255X/X}$ female mice may be useful in preclinical studies of potential therapeutic agents both as a clinically relevant outcome measure as well as a sensitive neurophysiological biomarker of treatment response. Future work is needed to determine whether these observed changes are consistent in other mouse models of RTT expressing different *MECP2* mutations.

Baseline EEG evaluation found increased delta power and decreased alpha power in *Mecp2*$^{R255X/X}$ mice in a brain-region sleep/wake state dependent pattern. Delta power was increased in the frontal area of MUT animals in all sleep/wake states, whereas delta power was only increased in the parietal region of MUT animals in the Wake state. Alpha power was decreased in the parietal region of MUT animals in Wake and NREM state, whereas this increase in alpha power in frontal region was observed in NREM and REM state. In both regions, changes in delta or alpha power was not seen in the MUT animals at the younger age. Elevation of delta power in MUT animals is consistent with similar observations in people with RTT (Ammanuel et al., 2015; Roche et al., 2019), with correlation to clinical severity in people with RTT. Thus, increased delta power has the potential to serve as a translational neurophysiological biomarker (Roche et al., 2019), but formal additional characterization and validation is needed. In the current study we were unable to detect a significant association between either delta or alpha power with severity of disease on MUT mice in postnatal age groups of 5–8 weeks and 20–24 weeks. This may be due to the limitation of the age ranges studied and the cross-sectional analysis performed, and future work is needed to further explore a potential correlation. However, we did see the negative correlation of the 1/f slope with phenotypic severity in parietal brain region. As the slope was calculated by the log-log transform of spectra between 2 and 24 Hz, the increased delta and decreased alpha power drive greater negative slope values, which implicates a change in the excitatory/inhibitory balance and potentially more asynchronized neural circuit network activity (Roche et al., 2019; Voytek et al., 2015). Moreover, similar correlation between 1/f slope and severity of disease has been reported in people with RTT (Roche et al., 2019). Thus, it would be promising to consider 1/f slope as a translational biomarker to predict disease progression. Finally, we observed a trend towards decrease in gamma power during REM in the parietal region and high gamma power during sleep state in the frontal region, which was similar to the previous results in *Mecp2*$^{Null/+}$ female animals (Wither et al., 2012), but was inconsistent with the results from male *Mecp2* $^{NULL/Y}$ or *Mecp2*$^{T158A/Y}$ male mice in waking condition (Goffin et al., 2012). These differential results might be

caused by the differences in animal gender, recording location or animal strain background between the studies. Thus far, information about parallel studies on people with RTT is lacking (Saby et al., 2020). Even though strong negative correlations between high gamma power and phenotypic severity were obtained, further evaluations looking at longitudinal progression in a variety of mouse models of RTT are needed to determine whether this feature could serve as a generalizable and translatable biomarker to guide preclinical or clinical studies.

Baseline EEG also identified spontaneous rhythmic epileptiform discharges in female *Mecp2*$^{R255X/X}$ mice, similar to those previously reported in female *Mecp2*$^{NULL/+}$ and male *Mecp2*$^{NULL/Y}$ mice (Lang et al., 2014; Wither et al., 2013; Wither et al., 2018). As convulsive seizures are a common clinical feature in people with RTT, future work will focus on prolonged video EEG recordings to evaluate convulsive seizure activity, and detailed characterization of changes in epileptiform discharge patterns during sleep/wake states longitudinally in the same animals over time. Interestingly, previous work showed that restoring MeCP2 expression or anti-seizure drug therapy in mouse models of RTT decreased the frequency of observed epileptiform discharges (Lang et al., 2014; Wither et al., 2018), pointing to potential utility as a biomarker in preclinical studies.

Event-related potentials are useful non-invasive methods to evaluate brain activity that can be associated with various behavioral and cognitive deficits and are valuable in neurodevelopmental conditions such as RTT in which there are limited methods to assess cognitive functioning. Critically, ERP methods can be developed and used across species, providing the ability to translate findings readily from preclinical studies to clinical trials. Within neurodevelopmental disorders, great progress has been made in Fragile X syndrome: parallel studies on ERP in people with Fragile X syndrome and preclinical animal models suggested that they could be employed as biomarkers to evaluate disease severity or predict treatment response (Ethridge et al., 2016; Ethridge et al., 2017; Ethridge et al., 2019; Lovelace, 2020; Sinclair et al., 2017b; Van der Molen et al., 2012; Wen et al., 2019). Previous work in people with RTT has found changes in both visual (LeBlanc et al., 2015) and auditory ERP (Stauder et al., 2006), and similar changes in both visual and auditory ERPs have been observed in mouse models of RTT (Durand et al., 2012; Goffin et al., 2012; Goffin et al., 2014). Importantly, Goffin et al. found that changes in AEP in male *Mecp2*$^{T158A/Y}$ mice is dependent on MeCP2 function in GABAergic neurons, supporting the idea that excitatory/inhibitory imbalance is a key feature in RTT (Goffin et al., 2014). In this study, we found decreased AEP peak amplitudes, increased peak latencies and decreased auditory stimulus-related power in female *Mecp2*$^{R255X/X}$ mice, similar to the results reported in people with RTT (Stauder et al., 2006) and in *Mecp2*$^{T158A/Y}$ mice (Goffin et al., 2012; Goffin et al., 2014). A previous study in female *Mecp2*$^{NULL/+}$ mice found the opposite effect, with increased N1 peak amplitudes of AEP and VEP (Liao et al., 2012). This discrepancy may reflect differences of recording locations. In the studies from Liao et al., two recording electrodes were placed into region CA1 of hippocampus, whereas our recordings were captured from dural electrodes above the cortex. Furthermore, other differences between the studies such as specific *MECP2* mutation, strain background, age, or other technical differences may have also contributed to the observed differences in our findings compared to Liao et al.; however we are reassured that

our findings our consistent with those observed in people with RTT and other published mouse studies. In brief, the correlation of auditory event-related potential and spectral power with disease severity suggests that these stimulation-related neurophysiological features could serve as biomarkers for RTT disease progression and potentially of disease improvement. The findings presented here of disrupted event-related phase locked power in *Mecp2*$^{R255X/X}$ female mice across a wide range of frequencies suggests alteration of long-range synchronization of neural activity occurred that might provide insight into neural circuit dysfunction underlying the development of specific phenotypic abnormalities.

Interestingly, EEG and AEP changes varied by brain region in these studies, pointing to spatial differences in neurophysiological function and stimulus response in RTT mice. A limitation in this work is the low number of EEG channels utilized here. Future work in mice using newer dense EEG electrode arrays (Jonak et al., 2018; Jonak et al., 2020) hold promise to further define brain regional differences, providing additional insight into the specific neural circuitry underlying abnormal response to auditory stimuli as well as additional opportunities to study long-range coherence in RTT mouse models.

In summary, this work identified a number of neurophysiological changes in a valid mouse model of RTT, female *Mecp2*$^{R255X/X}$ mice, that reproduce many neurophysiological features observed in people with RTT and in other mouse models of RTT. Importantly, the consistency of observed neurophysiological abnormalities between people with RTT and mouse models of RTT supports the translatable potential of these neurophysiological measures as meaningful biomarkers of disease progression or improvement. A limitation of this study is the cross-sectional nature, with only two age groups evaluated. Future work evaluating the developmental progression of these neurophysiological changes in individual animals, with an emphasis on the progression relative to the development of clinically relevant behavioral and neurophysiological phenotypes in each animal, will enhance the usefulness of these neurophysiological features as valid biomarkers. Additionally, the ability to genetically reverse RTT in mouse models (Guy et al., 2007) provides the opportunity to evaluate these neurophysiological features relative to phenotypic improvement. These neurophysiological features could also be incorporated into preclinical studies of novel therapeutics, as the translatability of these features from mouse to human can facilitate rapid movement between species. Finally, as other neurophysiological features have been found to be parallel in humans and mice in other neurodevelopmental disorders such as FXS (Ethridge et al., 2017; Ethridge et al., 2019; Lovelace et al., 2018; Lovelace, 2020; Wen et al., 2019), future evaluations of these in mouse models of RTT and people with RTT will be useful both to identify additional neurophysiological biomarkers and to help identify similarities and differences between neurodevelopmental disorders broadly.

Supplementary data to this article can be found online at https://doi.org/10.1016/j.nbd.2020.105083.

Supplementary Material

Refer to Web version on PubMed Central for supplementary material.

Acknowledgements

This work was supported by Eunice Kennedy Shriver Intellectual and Developmental Disabilities Research Center at Vanderbilt, U54HD083211 (JLN), HD083181 (JLN), and the Annette Schaffer Eskind Chair Fund. The content is solely the responsibility of the authors and does not necessarily represent the official views of the National Institutes of Health or the Eunice Kennedy Shriver Child Health and Human Development Institute (NICHD). Rodent experiments were performed in part through the use of the Murine Neurobehavior Core lab at the Vanderbilt University Medical Center.

References

Amir RE, et al. , 1999. Rett syndrome is caused by mutations in X-linked MECP2, encoding methyl-CpG-binding protein 2. Nat. Genet 23, 185–188. [PubMed: 10508514]

Ammanuel S, et al. , 2015. Heightened Delta power during slow-wave-sleep in patients with Rett syndrome associated with poor sleep efficiency. PLoS One 10, e0138113. [PubMed: 26444000]

Cuddapah VA, et al. , 2014. Methyl-CpG-binding protein 2 (MECP2) mutation type is associated with disease severity in Rett syndrome. J. Med. Genet 51, 152–158. [PubMed: 24399845]

D'Cruz JA, et al. , 2010. Alterations of cortical and hippocampal EEG activity in MeCP2-deficient mice. Neurobiol. Dis 38, 8–16. [PubMed: 20045053]

Durand S, et al. , 2012. NMDA receptor regulation prevents regression of visual cortical function in the absence of Mecp2. Neuron. 76, 1078–1090. [PubMed: 23259945]

Ellaway C, et al. , 2001. Sleep dysfunction in Rett syndrome: lack of age related decrease in sleep duration. Brain Dev. 23, S101–S103. [PubMed: 11738852]

Ethridge LE, et al. , 2016. Reduced habituation of auditory evoked potentials indicate cortical hyper-excitability in fragile X syndrome. Transl. Psychiatry 6, e787. [PubMed: 27093069]

Ethridge LE, et al. , 2017. Neural synchronization deficits linked to cortical hyper-excitability and auditory hypersensitivity in fragile X syndrome. Mol. Autism 8, 22. [PubMed: 28596820]

Ethridge LE, et al. , 2019. Auditory EEG biomarkers in fragile X syndrome: clinical relevance. Front. Integr. Neurosci 13, 60. [PubMed: 31649514]

Featherstone RE, et al. , 2015. Mice with subtle reduction of NMDA NR1 receptor subunit expression have a selective decrease in mismatch negativity: implications for schizophrenia prodromal population. Neurobiol. Dis 73, 289–295. [PubMed: 25461194]

Foxe JJ, et al. , 2016. Automatic cortical representation of auditory pitch changes in Rett syndrome. J. Neurodev. Disord 8, 34. [PubMed: 27594924]

Gandal MJ, et al. , 2010. Validating gamma oscillations and delayed auditory responses as translational biomarkers of autism. Biol. Psychiatry 68, 1100–1106. [PubMed: 21130222]

Gandal MJ, et al. , 2012. Gamma synchrony: towards a translational biomarker for the treatment-resistant symptoms of schizophrenia. Neuropharmacology. 62, 1504–1518. [PubMed: 21349276]

Glaze DG, et al. , 1987. Rett's syndrome: characterization of respiratory patterns and sleep. Ann. Neurol 21, 377–382. [PubMed: 3579223]

Goffin D, et al. , 2012. Rett syndrome mutation MeCP2 T158A disrupts DNA binding, protein stability and ERP responses. Nat. Neurosci 15, 274–283.

Goffin D, et al. , 2014. Cellular origins of auditory event-related potential deficits in Rett syndrome. Nat. Neurosci 17, 804–806. [PubMed: 24777420]

Guy J, et al. , 2007. Reversal of neurological defects in a mouse model of Rett syndrome. Science. 8, 8.

Johnson BS, et al. , 2017. Biotin tagging of MeCP2 in mice reveals contextual insights into the Rett syndrome transcriptome. Nat. Med 23, 1203–1214. [PubMed: 28920956]

Jonak CR, et al. , 2018. Reusable multielectrode array technique for electroencephalography in awake freely moving mice. Front. Integr. Neurosci 12, 53. [PubMed: 30416434]

Jonak CR, et al. , 2020. Multielectrode array analysis of EEG biomarkers in a mouse model of fragile X syndrome. Neurobiol. Dis 138, 104794. [PubMed: 32036032]

Key AP, Jones D, Peters S, 2019. Spoken word processing in Rett syndrome: evidence from event-related potentials. Int. J. Dev. Neurosci 73, 26–31. [PubMed: 30630072]

Lang M, et al. , 2014. Rescue of behavioral and EEG deficits in male and female Mecp2-deficient mice by delayed Mecp2 gene reactivation. Hum. Mol. Genet 23, 303–318. [PubMed: 24009314]

Laurvick CL, et al. , 2006. Rett syndrome in Australia: a review of the epidemiology. J. Pediatr 148, 347–352. [PubMed: 16615965]

LeBlanc JJ, et al. , 2015. Visual evoked potentials detect cortical processing deficits in Rett syndrome. Ann. Neurol 78, 775–786. [PubMed: 26332183]

Li Q, et al. , 2015. Circadian rhythm disruption in a mouse model of Rett syndrome circadian disruption in RTT. Neurobiol. Dis 77, 155–164. [PubMed: 25779967]

Liao W, et al. , 2012. MeCP2+/− mouse model of RTT reproduces auditory phenotypes associated with Rett syndrome and replicate select EEG endophenotypes of autism spectrum disorder. Neurobiol. Dis 46, 88–92. [PubMed: 22249109]

Light GA, Swerdlow NR, 2015. Future clinical uses of neurophysiological biomarkers to predict and monitor treatment response for schizophrenia. Ann. N. Y. Acad. Sci 1344, 105–119. [PubMed: 25752648]

Lovelace JW, et al. , 2016. Matrix metalloproteinase-9 deletion rescues auditory evoked potential habituation deficit in a mouse model of fragile X syndrome. Neurobiol. Dis 89, 126–135. [PubMed: 26850918]

Lovelace JW, et al. , 2018. Translation-relevant EEG phenotypes in a mouse model of fragile X syndrome. Neurobiol. Dis 115, 39–48. [PubMed: 29605426]

Lovelace JW, et al. , 2020. Deletion of Fmr1 from forebrain excitatory neurons triggers abnormal cellular, EEG, and behavioral phenotypes in the auditory cortex of a mouse model of fragile X syndrome. Cereb. Cortex 30 (3), 969–988. 10.1093/cercor/bhz141. [PubMed: 31364704]

McCauley MD, et al. , 2011. Pathogenesis of lethal cardiac arrhythmias in mecp2 mutant mice: implication for therapy in rett syndrome. Sci. Transl. Med 3, 113ra125.

Neul JL, et al. , 2008. Specific mutations in methyl-CpG-binding protein 2 confer different severity in Rett syndrome. Neurology. 70, 1313–1321. [PubMed: 18337588]

Neul JL, et al. , 2010. Rett syndrome: revised diagnostic criteria and nomenclature. Ann. Neurol 68, 944–950. [PubMed: 21154482]

Nomura Y, 2005. Early behavior characteristics and sleep disturbance in Rett syndrome. Brain Dev. 27 (Suppl. 1), S35–S42. [PubMed: 16182496]

Peters SU, Gordon RL, Key AP, 2015. Induced gamma oscillations differentiate familiar and novel voices in children with MECP2 duplication and Rett syndromes. J. Child Neurol 30, 145–152. [PubMed: 24776956]

Pitcher MR, et al. , 2015. Rett syndrome like phenotypes in the R255X Mecp2 mutant mouse are rescued by MECP2 transgene. Hum. Mol. Genet 24, 2662–2672. [PubMed: 25634563]

Roberts TP, et al. , 2010. MEG detection of delayed auditory evoked responses in autism spectrum disorders: towards an imaging biomarker for autism. Autism Res. 3, 8–18. [PubMed: 20063319]

Roche KJ, et al. , 2019. Electroencephalographic spectral power as a marker of cortical function and disease severity in girls with Rett syndrome. J. Neurodev. Disord 11, 15. [PubMed: 31362710]

Saby JN, et al. , 2020. Evoked potentials and EEG analysis in Rett syndrome and related developmental encephalopathies: towards a biomarker for translational research. Front. Integr. Neurosci 14, 30. [PubMed: 32547374]

Sinclair D, et al. , 2017a. GABA-B agonist baclofen normalizes auditory-evoked neural oscillations and behavioral deficits in the Fmr1 knockout mouse model of fragile X syndrome. eNeuro. 4.

Sinclair D, et al. , 2017b. Sensory processing in autism spectrum disorders and fragile X syndrome-from the clinic to animal models. Neurosci. Biobehav. Rev 76, 235–253. [PubMed: 27235081]

Smith C, 1996. Sleep states, memory processes and synaptic plasticity. Behav. Brain Res 78, 49–56. [PubMed: 8793037]

Stauder JE, et al. , 2006. The development of visual- and auditory processing in Rett syndrome: an ERP study. Brain Dev. 28, 487–494. [PubMed: 16647236]

Tarquinio DC, et al. , 2017. Longitudinal course of epilepsy in Rett syndrome and related disorders. Brain. 140, 306–318. [PubMed: 28007990]

Tarquinio DC, et al. , 2018. The course of awake breathing disturbances across the lifespan in Rett syndrome. Brain Dev. 40, 515–529. [PubMed: 29657083]

Uhlhaas PJ, Singer W, 2010. Abnormal neural oscillations and synchrony in schizophrenia. Nat. Rev. Neurosci 11, 100–113. [PubMed: 20087360]

Van der Molen MJ, et al. , 2012. Auditory change detection in fragile X syndrome males: a brain potential study. Clin. Neurophysiol 123, 1309–1318. [PubMed: 22192499]

Voytek B, et al. , 2015. Age-related changes in 1/f neural electrophysiological noise. J. Neurosci 35, 13257–13265. [PubMed: 26400953]

Wang J, et al. , 2017. A resting EEG study of neocortical hyperexcitability and altered functional connectivity in fragile X syndrome. J. Neurodev. Disord 9, 11. [PubMed: 28316753]

Ward KR, et al. , 2019. Src deficient mice demonstrate behavioral and electrophysiological alterations relevant to psychiatric and developmental disease. Prog. Neuro-Psychopharmacol. Biol. Psychiatry 93, 84–92.

Wen TH, et al. , 2019. Developmental changes in EEG phenotypes in a mouse model of fragile X syndrome. Neuroscience. 398, 126–143. [PubMed: 30528856]

Wither RG, et al. , 2012. Daily rhythmic behaviors and thermoregulatory patterns are disrupted in adult female MeCP2-deficient mice. PLoS One 7, e35396. [PubMed: 22523589]

Wither RG, et al. , 2013. Regional MeCP2 expression levels in the female MeCP2-deficient mouse brain correlate with specific behavioral impairments. Exp. Neurol 239, 49–59. [PubMed: 23022455]

Wither RG, et al. , 2018. Electrographic and pharmacological characterization of a progressive epilepsy phenotype in female MeCP2-deficient mice. Epilepsy Res. 140, 177–183. [PubMed: 29414525]

Young D, et al. , 2007. Sleep problems in Rett syndrome. Brain Dev. 29, 609–616. [PubMed: 17531413]

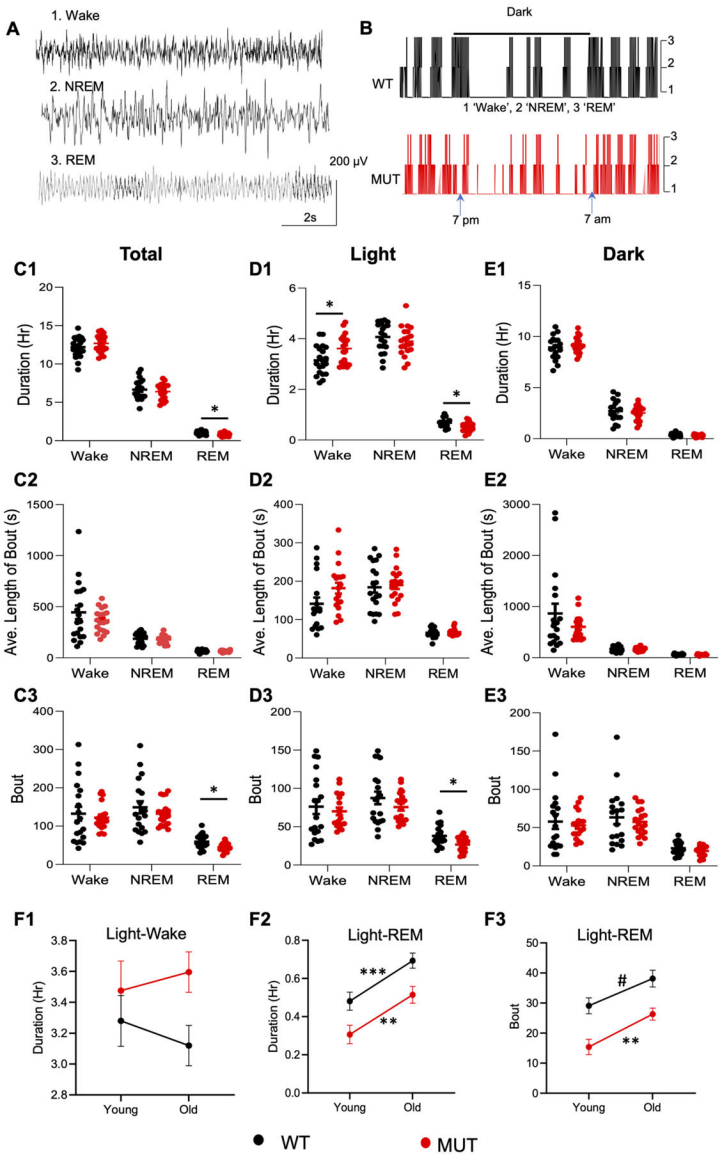

Fig. 1.

Quantitation of sleep/wake cycles in *Mecp2*$^{255X/X}$ female and WT controls. A. Representative EEG tracings showing animal activity state: 1. Wake, 2. NREM and 3. REM. B. Representative hypnogram for one WT and one MUT mouse. C-E. Individual value plot showing the difference between WT and MUT in total time durations, Average length of each bout and bout numbers of sleep/wake states in total observation period (C), light (D) and dark (E) cycle. *$p < 0.05$ significant difference between WT and MUT after Bonferroni correction on each parameter estimated in three sleep/wake states during dark, light and total observation period. Two tail unpaired *t*-test or Mann-Whitney *U* test used for bout numbers. F. Developmental changes of sleep duration in Wake (F1) and REM state (F2), as well as bout number in REM state in light cycle (F3). 'Young' means animal at age of 5–8 weeks and 'Old' means animal at age of 20–24 weeks. # $p < 0.1$, ** $p < 0.01$ and ***$p < 0.001$ between Young and Old. Two tail unpaired t-test used for duration and Mann-Whitney used

for bout number. Animal numbers throughout: WT $n = 11$, MUT $n = 10$ in Young group and WT = 18 and MUT = 18 in Old group.

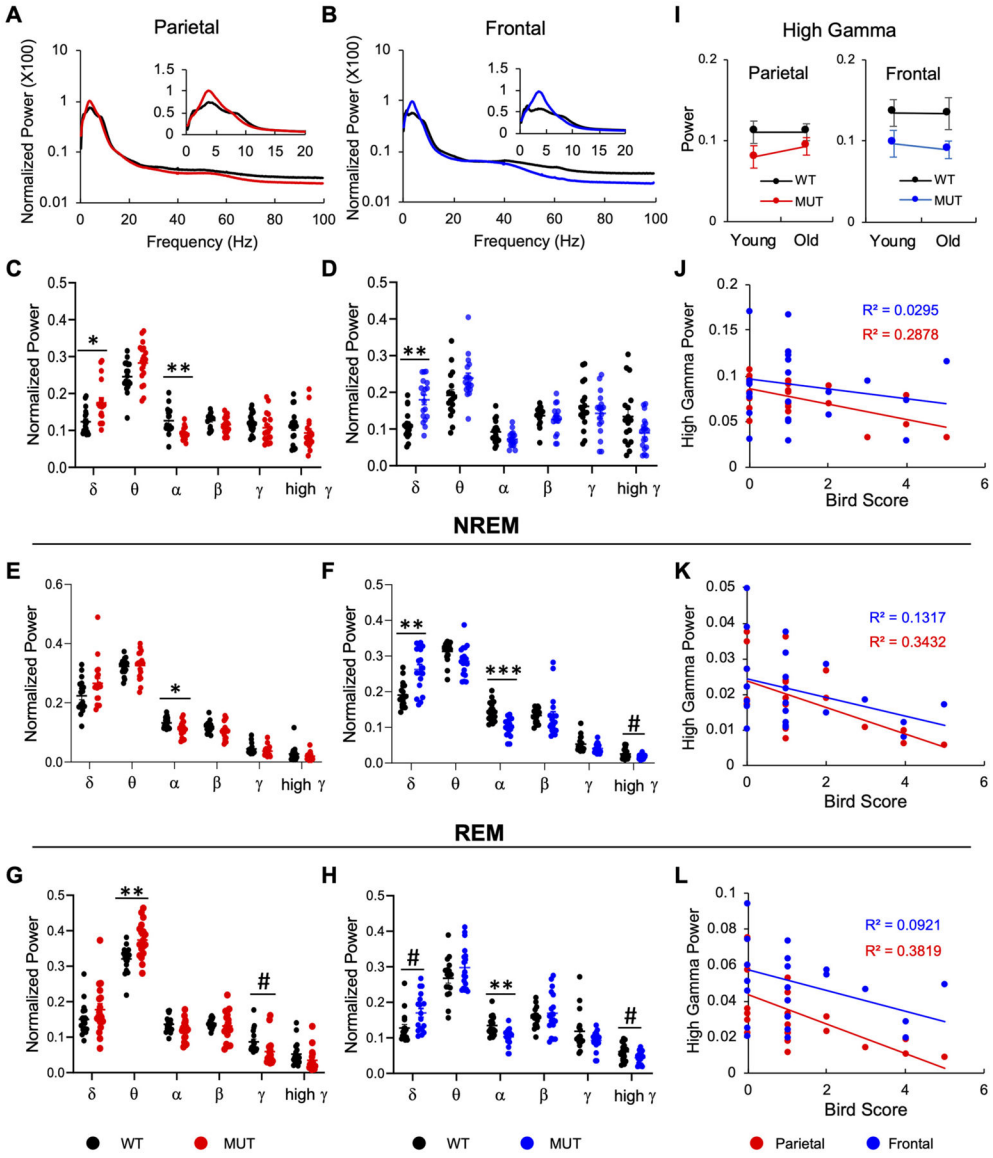

Fig. 2.

Basal EEG spectral power in *Mecp2* $^{R255X/X}$ female and WT controls. A and B. Normalized EEG power showing the mean spectra of Wake state between 0 and 100 Hz in logistic scale in parietal (A) and frontal (B) brain regions in animals at 20 to 24 weeks old. The insets show the normalized power between 2 and 20 Hz in normal scale. Data were normalized by the total power under the curve. C and D. Individual value plot showing each animal's spectral bands and means of delta (2–4 Hz), theta (4–8 Hz), alpha (8–12 Hz), beta (12–30 Hz), gamma (30–55 Hz) and high gamma power (65–100 Hz) in parietal region (n = 18 for both WT and MUT mice) and frontal region (n = 17 of WT and n = 18 of MUT). E and F. Same plot as C and D in NREM state. G and H. Same plot as C and D in REM state. I. Developmental change of high gamma power in parietal (left) and frontal (right) regions in wake state. Animal numbers in young group: WT (n = 11) and MUT (n = 10) in both brain regions. #p < 0.1, * < 0.05, ** p < 0.01, *** < 0.001 between WT and MUT, two

tail unpaired t-test with Bonferroni correction on 6 comparisons. J, K and L. Correlation between high gamma power and phenotypic severity during Wake (J, parietal: $p = 0.008$ and frontal: $p = 0.43$), NREM (K, parietal: $p = 0.003$ and frontal $p = 0.08$) and REM state, (L, parietal: $p = 0.002$ and frontal: $p = 0.16$). Spearman's analysis.

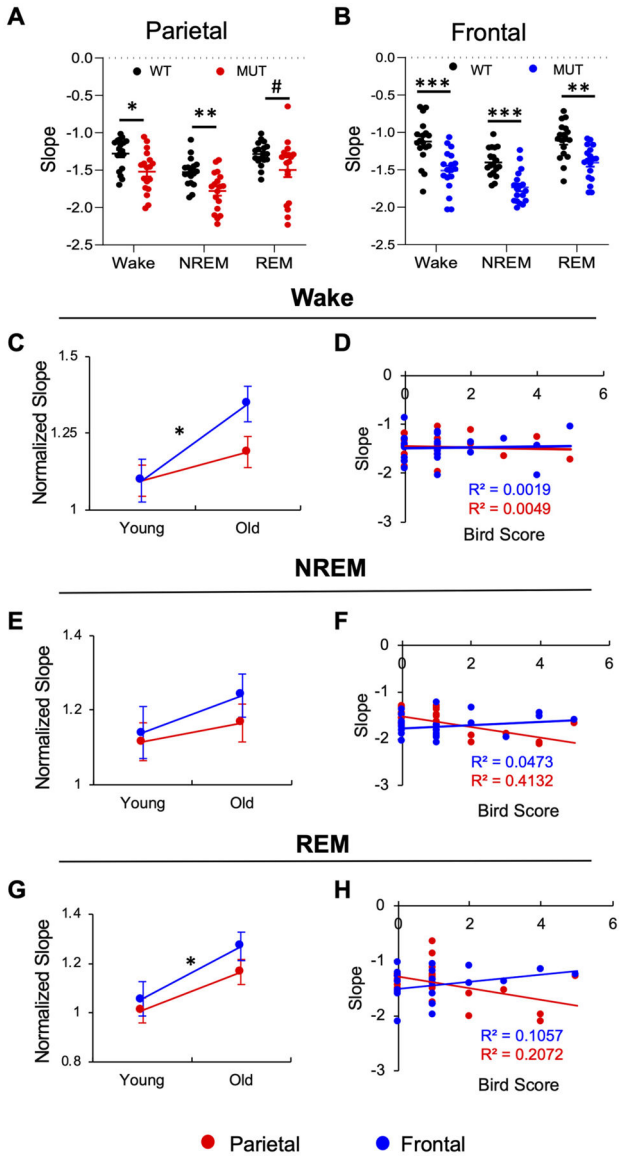

Fig. 3.

Slope of basal EEG spectral power in *Mecp2*$^{R255X/X}$ female and WT controls. A and B. Individual plot showing the difference of the 1/f slope between WT and MUT in Wake, NREM and REM state in both parietal (A) and frontal (B) regions at 20–24 weeks old. 1/f slope was estimated by the linear regression in log-log scale at the frequency range of 2–24 Hz. # < 0.1, * $p < 0.05$, **p < 0.01 and *** p < 0.001 between WT and MUT animals, two tail unpaired t-test with Bonferroni correction on three comparisons. C, E, G. Developmental changes of 1/f slope in both parietal (red) and frontal (blue) regions in the three sleep/wake state, Wake (C), NREM (E) and REM (G). Slope was normalized by the mean of slope in WT animals in both Young and Old groups. * p < 0.05, Young vs. Old, two tail Mann-Whitney U test. D, F, H. Correlation between 1/f slope and phenotypic severity in parietal (red) and frontal (blue) regions during Wake (D), NREM (F) and REM (H) state.

Significant correlation was seen in the parietal region during NREM (p = 0.003) and REM (p = 0.02) state, Spearman's analysis. Animal numbers are the same as in Fig. 2.

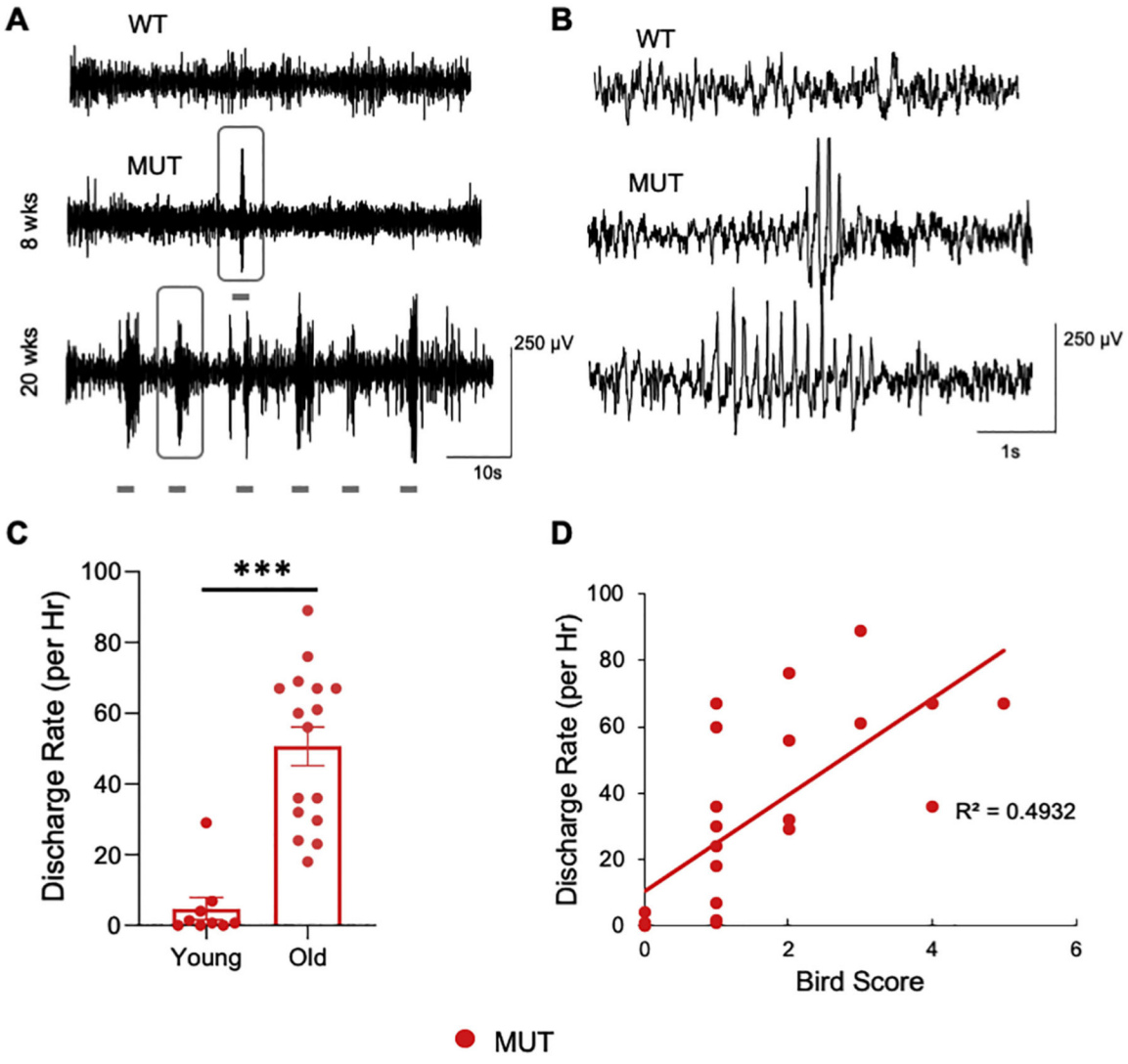

Fig. 4.

Epileptiform discharges characterized in *Mecp2*$^{R255X/X}$ female mice. A and B. Examples of epileptiform discharges at young and old age in expanded time scale (A) and shorter time scale (B) enlarged from rectangle box in A. C. Epileptiform discharge rate calculated by number of discharges per hour from individual mutant animals at young (n = 9) and old age (n = 16). *** p < 0.001, Young vs. Old, two tail Mann-Whitney test. D. Correlation between epileptiform discharge rate and phenotypic severity in mutant animals, p = 0.002, Spearman's analysis.

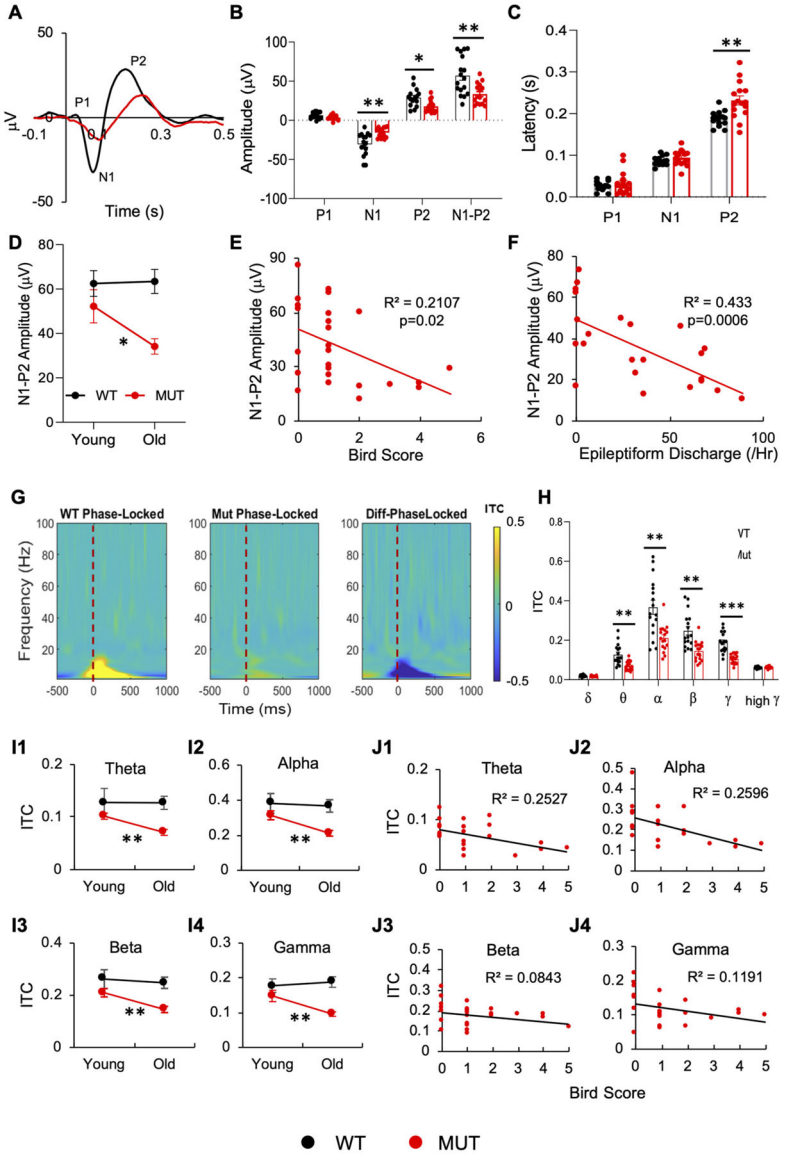

Fig. 5.

Auditory event-related potential evoked in parietal cortex of *Mecp2* $^{R255X/X}$ female and WT controls. A, B and C. AEP evoked in WT and MUT animals at age of 20–24 weeks. A. Grand average ERPs obtained from animal's response to 200 broadband white noise (5–40 kHz) stimulation. P1, N1, and P2 were defined as maximum or minimum voltage deflections within 10–70 ms, 50–150 ms, or 100–350 ms, respectively. AEP amplitudes (B) and latency (C) between WT (n = 16) and MUT (n = 16) mice. * $p < 0.05$ and ** $p < 0.01$ WT vs. MUT, two tail unpaired t-test with Bonferroni correction on 4 comparisons for amplitude and 3 comparisons for latency. D. Developmental changes of N1-P2 amplitude in both WT and MUT animal. * $p < 0.05$, Young vs. Old, two tail unpaired t-test. Animal number in Young group, WT (n = 9) and MUT (n = 10). E, F. Correlation between AEP N1-P2 amplitude and phenotypic severity (E, $p = 0.02$) and epileptiform discharge (F, $p = 0.0006$), Spearman's analysis. G. Time-frequency plots showing inter-trial coherence in

response to sound stimulation in a WT (left) and MUT (middle) mouse and the difference in phase-locked power MUT-WT (right). H. Individual plots showing the difference of ITC between WT and MUT at each power band. **p < 0.01 and *** p < 0.001, two tail unpaired t-test with Bonferroni correction by 6 comparisons. I. Developmental changes of inter-trial phase coherence at theta (I1), alpha (I2), beta (I3) and gamma (I4) power bands. * p < 0.05, Young vs. Old, two tail unpaired t-test. J. Correlation between ITC at individual power bands and phenotypic severity (Bird score). Significant correlation was found at theta (J1, $p = 0.017$) and alpha (J2, $p = 0.015$) but not beta (J3, $p = 0.179$) and gamma (J4, $p = 0.112$), Spearman's analysis.

Table 1

Wake and sleep characteristics in R255X female mice at postnatal age of 5–8 weeks.

		Duration (Hrs)			Ave. Length of Bout (s)			Bout Number		
		WT	**Mut**	**p adj.**	**WT**	**Mut**	**p adj.**	**WT**	**Mut**	**p adj.**
Dark	Wake	9.10 ± 0.14	9.00 ± 0.32	> 0.99	449.5 ± 75.1	598.3 ± 63.2	0.132	55.5 ± 5.8	39.4 ± 4.9	0.1266
	NREM	2,62 ± 0.12	2.72 ± 0.29	> 0.99	177.4 ± 15.9	249.1 ± 28.3	0.1722	57.9 ± 5.7	43.5 ± 5.7	0.1558
	REM	0.28 ± 0.03	0.27 ± 0.04	> 0.99	57.7 ± 2.9	67.5 ± 4.0	0.1374	16.8 ± 1.9	15.0 ± 2.2	0.5187
Light	Wake	3.28 ± 0.17	3.47 ± 0.20	> 0.99	174.2 ± 18.5	241.3 ± 16.0	0.0972	69.7 ± 7.6	49.5 ± 4.4	0.1392
	NREM	3.97 ± 0.20	3.99 ± 0.21	0.9497	202.2 ± 19.3	273.7 ± 24.9	0.1518	75.3 ± 6.4	55.6 ± 4.0	0.0966
	REM	0.48 ± 0.05	0.31 ± 0.05	0.1674	58.9 ± 3.3	74.5 ± 6.0	0.1712	29.1 ± 2.8	15.4 ± 2,7	0.0135 *
Total	Wake	12.4 ± 0.2	12.5 ± 0.4	> 0.99	367.1 ± 35.4	452.5 ± 31.7	0.1592	125.2 ± 12.8	88.9 ± 6.6	0.1095
	NREM	6.59 ± 0.21	6.71 ± 0.33	> 0.99	194.7 ± 16.4	255.3 ± 22.4	0.1196	133.2 ± 11.3	99.1 ± 6.8	0.1116
	REM	0.76 ± 0.06	0.58 ± 0.08	0.6144	60.3 ± 1.9	70.2 ± 4.2	0.135	45.9 ± 3.8	29.4 ± 3.5	0.0272 *

* $p < 0.05$ WT vs. MUT Mann-Whitney U test with Bonferroni-Holm correction.

Table 2

Basal EEG power in R255X female mice at postnatal age of 5–8 weeks.

		Parietal			Frontal		
		WT	**Mut**	**p adj.**	**WT**	**Mut**	**p adj.**
Wake	Delta	0.13 ± 0.01	0.14 ± 0.01	0.5982	0.14 ± 0.01	0.16 ± 0.01	0.7143
	Theta	0.23 ± 0.02	0.28 ± 0.02	0.1464	0.17 ± 0.01	0.21 ± 0.01	0.1524
	Alpha	0.09 ± 0.01	0.09 ± 0.01	0.5298	0.06 ± 0.00	0.06 ± 0.00	0.8257
	Beta	0.12 ± 0.01	0.12 ± 0.01	0.6137	0.11 ± 0.01	0.11 ± 0.01	> 0.99
	Gamma	0.10 ± 0.01	0.09 ± 0.01	0.3988	0.12 ± 0.01	0.09 ± 0.01	0.5048
	High Gamma	0.11 ± 0.01	0.08 ± 0.01	0.299	0.13 ± 0.02	0.10 ± 0.02	0.479
NREM	Delta	0.17 ± 0.01	0.19 ± 0.01	0.5943	0.17 ± 0.01	0.21 ± 0.01	0.063
	Theta	0.28 ± 0.02	0.32 ± 0.02	0.755	0.29 ± 0.01	0.28 ± 0.01	0.8538
	Alpha	0.11 ± 0.01	0.11 ± 0.01	0.6594	0.11 ± 0.01	0.08 ± 0.01	0.0642
	Beta	0.13 ± 0.01	0.11 ± 0.01	0.3432	0.11 ± 0.01	0.09 ± 0.01	0.3038
	Gamma	0.05 ± 0.01	0.04 ± 0.01	0.7284	0.05 ± 0.01	0.04 ± 0.01	0.1312
	High Gamma	0.04 ± 0.01	0.03 ± 0.01	0.6038	0.04 ± 0.01	0.03 ± 0.01	0.3936
Rem	Delta	0.13 ± 0.01	0.14 ± 0.01	> 0.99	0.13 ± 0.01	0.17 ± 0.01	0.7524
	Theta	0.29 ± 0.02	0.34 ± 0.02	0.1704	0.25 ± 0.01	0.26 ± 0.01	0.9648
	Alpha	0.11 ± 0.01	0.11 ± 0.01	> 0.99	0.09 ± 0.01	0.08 ± 0.01	0.6905
	Beta	0.13 ± 0.01	0.12 ± 0.01	0.9208	0.11 ± 0.01	0.10 ± 0.01	0.5961
	Gamma	0.08 ± 0.01	0.07 ± 0.01	0.252	0.10 ± 0.01	0.07 ± 0.01	0.7176
	High Gamma	0.06 ± 0.01	0.95 ± 0.01	0.9567	0.08 ± 0.01	0.06 ± 0.01	0.9747

p was adjusted by Bonferroni-Holm method.

Table 3

AEP in R255X Female Mice at Postnatal Age of 5–8 Weeks.

		Parietal			Frontal		
		WT	**Mut**	**p adj.**	**WT**	**Mut**	**p adj.**
Amplitude (uV)	P1	4.68 ± 1.17	4.71 ± 0.90	> 0.99	1.56 ± 1.18	5.28 ± 1.91	0.1351
	N1	−44.43 ± 6.95	−22.34 ± 4.69	0.0508	−31.96 ± 6.2	−10.40 ± 2.58	0.0084 **
	P2	37.06 ± 5.93	21.67 ± 4,58	0.0992	26.16 ± 5.13	9.65 ± 2.37	0.0086 **
	N1-P2	80.35 ± 11.34	48.57 ± 8.76	0.1551	62.63 ± 11.25	24.44 ± 4.9	0.0102 *
Latency (s)	P1	0.04 ± 0.01	0.03 ± 0.01	0.8103	0.04 ± 0.01	0.05 ± 0.01	0.1066
	N1	0.09 ± 0.01	0.1 ± 0.01	0.7584	0.09 ± 0.00	0.11 ± 0.01	0.0051 **
	P2	0.18 ± 0.01	0.23 ± 0.02	0.0537	0.17 ± 0.00	0.24 ± 0.02	0.0003 ***

* $p < 0.05$.

** $p < 0.01$.

*** $p < 0.001$ two-tail unpaired t-test with Bonferroni-Holm correction.